Spin Condensates in Semiconductor Microcavities

Jeremy J. Baumberg†

1 Introduction

Direct-gap semiconductors interact extremely strongly with light, absorbing energy in the promotion of electrons into the conduction band. The lifetime of the photoexcited electrons is several nanoseconds, set by competing processes of radiative and non-radiative recombination. Of increasing interest in the last decade, is the *phase* of the photoexcited electrons (or the *interband coherence*) induced by the oscillating optical field (Fig. 1). The time for this phase memory to be lost is much shorter than the carrier lifetime, typically less than 100 fs in bulk materials at room temperature, and is controlled by the range of possible phase scattering events accessible to the carriers. By freezing out the lattice vibrations at low temperatures, and quantum confining the carriers in volumes smaller than their de Broglie wavelengths, it is possible to reduce the phase scattering. Such confinement produces quasi-atomic energy levels whose separation restricts the events that can cause phase scattering. However even in fully-confining semiconductor quantum dots at liquid helium temperatures, the phase decay is only slowed by a factor of 200 [1]. Thus although such quantum dot systems have been suggested as all-solid-state elements for quantum computing applications, they are still prone to dephasing events which cause errors.

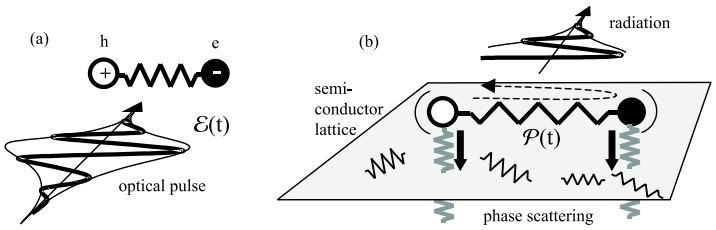

Fig. 1. (a) Optical pulse incident on a semiconductor creates an interband polarization $P(t)$ of Coloumb-bound electrons and holes which can (b) decay by reradiation, or phase scattering with a material excitation

In this chapter we will explore the potential of an alternative semiconductor quantum system that displays some startling features with the capabil-

ity to enhance electronic phase memories. Although superficially similar to conventional semiconductor heterostructures, we will show how this system can produce radically different properties, one of which is a phase lifetime in excess of many nanoseconds. The extra ingredient employed is the *strong* coupling of light and matter, which can lead to peculiar quantum behaviours, as in quantum electrodynamics atom-cavity experiments such as micromasers [2,3]. In semiconductors, strong coupling mixes the photon and electronic excitations so completely that it becomes impossible to distinguish them. Instead quasiparticles built from their mixture become the new basis states, and their properties can differ considerably from those of their components. Thus it is possible to induce new properties for photoexcited electronic states in a semiconductor which open up alternative routes for coherent control and quantum coherent technologies. In Section 2 we will outline the origin of the strong coupling regime, and discuss the properties of these quasiparticles termed *polaritons*. An exhaustive review of polariton properties is beyond the scope of this chapter and the reader is referred to recent reviews [4,5]. Experimental evidence recently reported for the interactions between these quasiparticles is summarized in Section 3. This leads to a discussion in Section 4 of the properties of such quasiparticles at high densities, and predicts a new type of quasiparticle condensate analogous to Bose-Einstein atomic condensates. We then set out the evidence for this polariton condensate, and discuss how it might be usefully manipulated.

2 Polariton Properties

2.1 Strongly-coupled microcavity dispersion

When atoms emit light in a high-finesse cavity which is tuned to the same frequency as the atomic transition, the emission process changes its character. The enhanced electric field can stimulate emission even with only one photon in the cavity, however the photon has a strong probability of being reabsorbed. Energy can cycle repeatedly between atom and cavity field, at a rate known as the Rabi frequency which is determined by the atomic oscillator strength. With the advance of semiconductor epitaxy, it has become possible to devise monolithic solid samples which exhibit the same cyclic interplay between light and matter. Typical samples consist of two high reflectivity mirrors (composed of semiconductor multilayers) separated by a cavity of a thickness roughly the size of the optical wavelength in the material ($d \sim 250\,\mathrm{nm}$). Embedded within this microcavity are a number of semiconductor quantum wells (QWs) at positions at which the resonant cavity electric fields are maximised. The oscillator strength of quantum wells is particularly large because the electron-hole pairs that can be photoexcited are bound together by the Coulomb interaction into excitons, which are further stabilised by the confined 2D planar geometry. In the samples we discuss,

it is these excitons which dominate the optical response near the bandgap of the semiconductor. The most important condition engineered into these devices is that the emission wavelength of the excitons matches the resonant wavelength of the microcavity. At low temperatures, such a sample (shown schematically in Fig. 2) allows the cycling between light and exciton to become faster than both the phase scattering of the individual excitons and the photon decay from the cavity, and hence the strong coupling regime is attained.

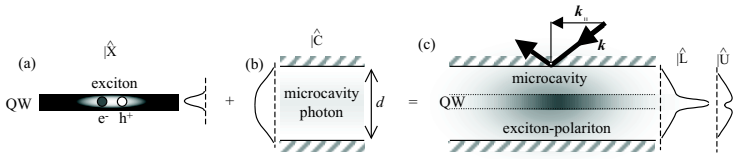

Fig. 2. Schematic wavefunctions of (a) exciton in a quantum well (QW), thickness $\simeq 10\,\mathrm{nm}$ (b) cavity photon in a microcavity, thickness $\simeq 250\,\mathrm{nm}$ (c) microcavity polariton. Light impinging at angle of incidence θ has in-plane momentum, $k_\parallel$

The new quasiparticles, called 'exciton-polaritons' (henceforth abbreviated as polaritons), are mixtures of the cavity photon $|\hat{C}\rangle$, and exciton $|\hat{X}\rangle$ bases, given by

$$\begin{bmatrix} \hbar\omega_x & \hbar\Omega \\ \hbar\Omega & \hbar\omega_c \end{bmatrix} \begin{bmatrix} |\hat{X}\rangle \\ |\hat{C}\rangle \end{bmatrix} = E \begin{bmatrix} |\hat{X}\rangle \\ |\hat{C}\rangle \end{bmatrix} \tag{1}$$

The Rabi coupling strength, Ω, produces an anticrossing between the energies of cavity photon ω_c and exciton $\omega_x = \omega_0 + \frac{\hbar k^2}{2m_x}$ (where the minimum exciton energy ω_0 is several meV binding energy below the semiconductor band gap). At normal incidence, the detuning of the cavity from the exciton, $\Delta = \omega_c - \omega_x = 0$, and the two polariton branches (upper and lower) have equal admixtures of light and matter, $|\hat{L}\rangle = \frac{1}{\sqrt{2}}(|X\rangle + |C\rangle), |\hat{U}\rangle = \frac{1}{\sqrt{2}}(|X\rangle - |C\rangle)$. It is important to note that this mixing changes as the angle of incidence onto the planar heterostructure changes, which corresponds to increasing the in-plane momentum, $k_\parallel = \omega \sin\theta/c$. The origin of this angular dispersion is the increase of cavity resonant frequency at increasing angles of incidence, $\omega_c = (\omega_0 + \Delta)\sqrt{1 + (k_\parallel/k_z)^2} \simeq (\omega_0 + \Delta)(1 + k_\parallel^2/2k_z^2)$ caused by the condition that the photon momentum perpendicular to the cavity must remain fixed, $k_z = 2\pi/d$. The exciton, being a much heavier particle, acquires little in-plane kinetic energy at these small momenta and thus the detuning between exciton and cavity modes increases as $k_\parallel$ increases, leading to their decoupling at angles greater than about 40° (Fig. 3). The two polaritons can be readily observed as strong dips in the near 100% reflectivity of the cavity mirrors, or as twin peaks in the sample transmission centered at $\omega_L = \omega_x - \Omega,\ \omega_U = \omega_x + \Omega$.

The strength and position of each peak matches well with this model of coupled oscillators.

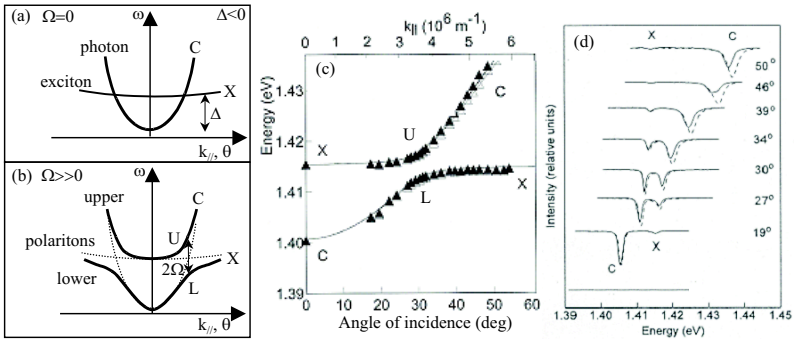

Fig. 3. In-plane dispersion relations at $\Delta \simeq -15\,\mathrm{meV}$ for (a) cavity photons and excitons without interactions, and (b) coupled polaritons (c) Measured angular dispersion and transfer-matrix fit for TE/TM polarizations. (d) Reflectivity spectra for TE/TM at different angles of incidence (data courtesy of R.M. Stevenson)

Polariton traps

The dispersion relation for the polaritons mapped in Figure 3b is critical for understanding the polariton interactions and merits further discussion. For $\Delta = 0$, the two polariton states are energetically split equally around the original energies by the Rabi frequency $\hbar\Omega = \sqrt{nf/2\varepsilon m_x d}$ where n QWs of oscillator strength per unit area, $f \sim 8/\pi a_0^2 \sim 6.10^{12}\,\mathrm{cm}^{-2}$, are embedded in a microcavity of dielectric constant ε. As the cavity mode disperses strongly upwards in energy at greater angles, the exciton becomes less mixed in and tends to its unperturbed value. This leads to the formation of a *polariton trap* in momentum space of depth Ω and momentum HWHM, $\Delta k \simeq \sqrt{3\varepsilon\omega_x\Omega}/c$ [6]. A near-stationary exciton can emit half a photon into the cavity producing an electric field which interferes with the electron-hole polarization, and leading to a decrease in the total electromagnetic energy for the lower polariton branch $|\hat{L}\rangle$. Such a trap is rather different to magnetic or *rf* atomic traps which exist in real space. Instead it resembles a 'kinetic' trap for a macroscopic particle, because the lowest energy state has the particle at rest, to which it returns due to frictional dissipation. The polariton is very light in comparison to the exciton mass ($m_L = 4\pi^2\hbar/\omega_0 d^2 \sim 10^{-5} m_e$ [5]) so the trap is narrow and deep which encourages the polaritons to come to a *complete* standstill. The sequestration of polaritons in a trap near $k = 0$ of lower energy than the huge reservoir of exciton states is the origin of the

dramatic reduction in their phase scattering, since far few interactions are available to polaritons than to excitons.

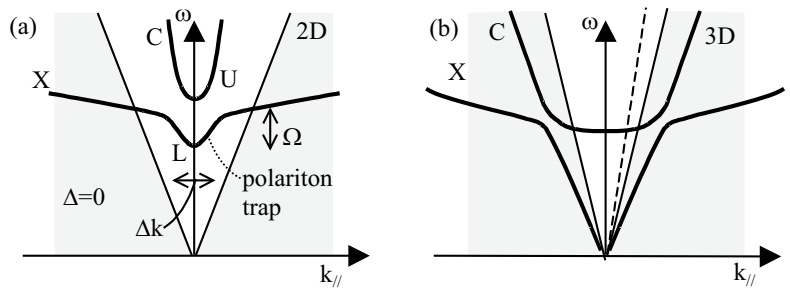

Fig. 4. In-plane dispersion relation for (a) 2D planar QW microcavity polaritons with strong coupling at k=0, and (b) 3D bulk polaritons. Only non-shaded regions have photon wavevectors accessible from outside the sample. The dashed line marks wavevectors at a nonzero angle of incidence

From this dispersion, we can also note that exciton-polaritons in microcavities possess a number of advantages to the experimentalist over their counterparts in bulk semiconductors. The first is that while all polariton coupling in bulk 3D samples exists at k outside the light cone (Fig. 4), when the symmetry is broken by the planar cavity the resonant region is now easily accessible by externally impinging light. This enables us to study predictions of polariton dynamics made several decades ago [7] but now accessible directly. Previous experiments on bulk systems mapped the polariton dispersion and observed 'hyper-Raman' scattering of small magnitude which required extremely high optical intensities [8]. While bulk semiconductors convert polaritons to light in a 'dead-layer' close to the sample surface (whose character is still under discussion [9]), in 2D the semiconductor microcavities can be engineered for highly-specific light-matter interactions. Finally, no comparable trap exists within the 3D polariton dispersion, although it does possesses many discrete states near the resonance with varying light-matter mixtures [10].

Wavefunction annealing

Our discussion of polariton dispersion relations makes a big assumption, that the in-plane momentum of each quasiparticle is a well-defined quantum number. This turns out to be true only because of the strong coupling of photon and exciton which forms the polariton trap. To see this, two extra perturbations must be considered to our simple picture of excitons: the Coulomb interaction between charged carriers, and disorder from imperfect crystalline growth. For low-energy excitons lying in local troughs of the potential energy, the disorder implies that the basis states for the center of mass motion

of the excitons are not plane waves, but localised states instead. However, as long as the light-matter coupling is strong enough, it can pull out parts of each localised wavefunction to make a polariton with a much large lateral extent than the localised states. In order words, different localised excitons couple to each other by exchanging photons which diffract laterally in the planar cavity. A very similar process can occur for vertically stacked quantum wells [11]. This photon-induced delocalisation produces polaritons which are very different from their component excitons through a sort of wavefunction *annealing*, with a lateral extent no longer limited by the local potential fluctuations or alloy disorder inherent in the semiconductor epitaxy (Fig. 5). In planar microcavities, the lateral coherence length $l_c = \sqrt{8\lambda_x dF} \sim 50\,\mu$m where the finesse $F \sim 1000$ [12]. Such states are thus macroscopic quantum objects (and can be resolved with the naked eye!) however they may also be much smaller (Section 4).

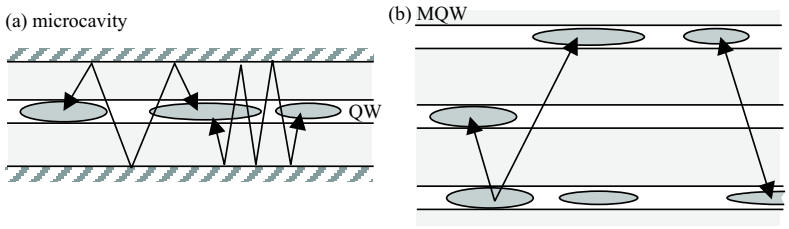

Fig. 5. Schematic wavefunction 'annealing' for polaritons arising from photon-mediated interactions of localised excitons spaced (a) laterally in a 2D planar microcavity, (b) vertically within different multiple quantum wells (MQWs)

The second perturbation which should be included is the Coulomb interaction between the electron and holes that make up excitons, which also couples together quasiparticles at different $k_\parallel$. The true ground state description must be a many-body wavefunction (as discussed by many theoretical groups [4,13–17]), with some similarity to a metallic or superconducting ground state, and further complicated by the non-equilibrium situation often set up in practice. In the weak coupling regime in which the mutual repulsion of $|\hat{X}\rangle$ and $|\hat{C}\rangle$ is less than the exciton linewidth, there is no polariton trap and the excitons are virtually degenerate. In this situation in which the Coulomb interaction can couple together a huge number of states exceeding the optical spectroscopy window ($k_\parallel > \omega/c$), it is hard to make a case for the exciton momentum being a good quantum number. Only when the polaritons form in a trap in which they are energetically below almost all states in the sample, is the Coulomb scattering suppressed and we can plausibly refer to in-plane momentum. Experimentally this is confirmed by the observation of local populations at distinct $k_\parallel$ for microcavities, but a virtually instanta-

neous spread to all $k_{\|}$ when quantum well excitons are excited with a specific momentum.

2.2 Polariton dynamics and Pair Scattering

With an understanding of the dispersion relation for polaritons in these planar structures, we can return to a question which motivated much of our research: *To what extent do polaritons represent a simple linear superposition of half an exciton and half a photon, and to what extent are their properties indicative of a new particle?* The answer to this depends on the properties of interest, since linear spectroscopy of semiconductor microcavities solely measures the mixed linear dispersion relation [4,5]. However almost any other optical property involves extra interactions of polaritons, such as the relaxation of polaritons to produce photoluminescence or nonlinear optical absorption and emission. In this section we summarize why polariton interactions are so different to the well-known properties of excitons. Such differences are important since the interaction of electrons, holes, and light is the basis for the engineering of semiconductor lasers, amplifiers and optoelectronic switches.

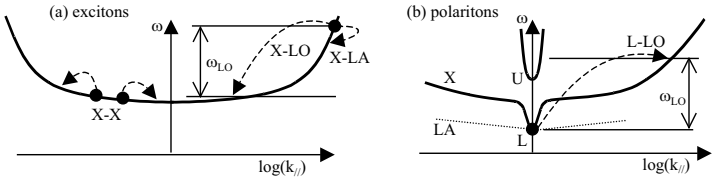

Fig. 6. In-plane dispersion relation and interactions of (a) excitons, and (b) polaritons with QW excitons. Optic phonon interactions (X-LO) involve large energy changes as compared with acoustic phonon scattering (X-LA). Exciton-exciton scattering (X-X) is allowed over a broad energy range. The dotted line marks the acoustic phonon dispersion, which shows the lack of available final states for polaritons in the trap absorb heat

Excitons interact most strongly with longitudinal optical (LO) phonons which in GaAs have an energy $\omega_{LO} = 36\,\mathrm{meV}$, and at high density excitons interact strongly with each other. A heated population of excitons also cools by acoustic phonon emission on rather longer timescales ($\sim 100\,\mathrm{ps}$). Simple considerations of energy-momentum conservation allow us to see that all three processes are very different for polaritons (Fig. 6). Polaritons within the trap have a number of pair scattering interactions which will be discussed later. However it is difficult for polaritons in the trap to escape by absorbing acoustic phonons at these temperatures because this does not provide enough energy to get them out in a single event. Only if the sample is hot enough so that there are enough of the energetic LO phonons, or enough hot excitons available, do polaritons get ionized out of their trap [6,18]. These

restricted scatterings produce the particular stability of polaritons compared to excitons, even if there is a large density of polaritons excited in the trap.

Besides the energetic separation of polaritons and excitons produced by the strong coupling, one of the other key properties introduced is the change in *shape* of the dispersion relation. Both the exciton and cavity photon mode dispersions are quadratic at small k, which precludes any direct non-trivial pair scattering since both energy and momentum cannot be conserved. Only through the existence of unbound states of the electron and hole can Coulomb scattering between QW excitons occur, as they can take up the extra momentum. The distorted S-shape of the lower polariton dispersion is responsible for turning on a whole new array of interactions which can be observed experimentally.

3 Experiments

3.1 Experimental setup

Since the discovery of strong coupling in semiconductor microcavities [19], most experiments have concentrated on absorption or photoluminescence with non-resonant continuous-wave photoexcitation. As discussed above, this allows accurate mapping of the in-plane dispersion relation, but produces a confused picture as regards the interaction of polaritons on their dispersion curve. One key advance has been to examine the dynamics of the polaritons using pulsed excitation. This allows us to locate the products of scattering at different points along the dispersion curve, by spectroscopically probing the sample at different angles of incidence. It also allows a study of how scattering controls phase relaxation. Here we describe our experiments devised to carry out this program of research. A number of groups have now performed experiments which substantially confirm the picture described below, and also extend it further [20–25].

To ensure laser pulses arrive at the sample at the same time regardless of their angle of incidence, a femtosecond goniometer must be constructed (Fig. 7). Experimentally we find maximum temporal shifts on the order of 100 fs (irrelevant for results presented here with 3 ps pulses), caused by imperfect realignment and systematic deviations through the optical windows of the cryostat and the sample substrate. In pump-probe experiments, one arm is kept fixed while the other is rotated allowing simple realignment on the same sample location. The goniometer-cryostat configuration is so constructed as to allow a very wide angular field of view ($\pm 70^\circ$) on both the front and back of the sample, allowing simultaneous measurement of reflection and transmission.

Because spectroscopic measurements are needed along the dispersion curve, the wavelength and spectral bandwidth of the pulses must be carefully controlled to match that of the polaritons. The main problem is to produce synchronized pulses of different colour. This is solved by using a short-pulse

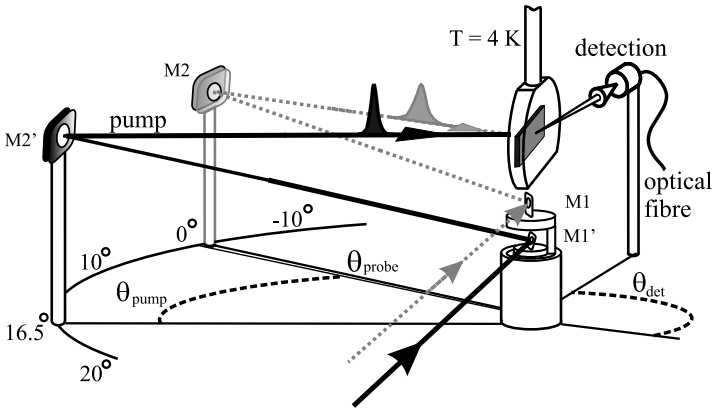

Fig. 7. Femtosecond goniometer: Each laser beam is first directed to a $\frac{1}{2}$" mirror (M1) which is placed directly underneath the sample, and is able to rotate about a vertical axis. The beam emerges from this mirror along the direction intended as the angle of incidence and arrives at a mirror (M2) at the same height as the sample, on the end of an arm which can rotate about the same vertical axis through the sample. This final mirror then directs the beam to the sample through a 20cm focal length lens. To change the angle of incidence, the arm is set to the correct angle of incidence and M1 rotated to redirect the beam back onto M2. The total path length to the sample is preserved and thus the arrival time is unchanged

Ti:sapphire laser with a wide spectral bandwidth (10 nm) from which the desired pulses can be excised, as developed for coherent control spectroscopies [26]. The basic method is to spatially separate the different colours in the pulse using a diffraction grating and bring them to a focus at a modulator plane. Here a computer-controlled liquid-crystal spatial light modulator allows control of both the amplitude and phase of each colour transmitted, before the pulse is reassembled at a matched diffraction grating. Sophisticated software allows calibration and selection of any desired pulse shape or sequence, with any spectral content contained in the original laser pulse. Such an arrangement in both pump and probe beamlines allows independent tuning in wavelength, pulse-length and pulse-shape. Finally we both spectrally- and temporally-resolve the combined emission/probe transmission at any angle, using rapid-scan time-delay stages, high-frequency lock-in detection and optical fibre to convey the light to a monochromator and cooled CCD system.

The combination of these techniques rapidly produces large data sets containing signatures of the interaction processes. In addition, a number of other important degrees of freedom are explored including the power of pump and probe pulses, and their polarization state. Both these are computer-controlled using liquid-crystal waveplates and Glan-laser polarizers. The electric-field polarization in the sample depends on the angle of incidence, and care must be taken to compensate for Fresnel losses and phase shifts in the final approach arm to the sample. The purity of circular polarization is confirmed by

the suppression by $> 30\,\mathrm{dB}$ of interactions from opposite circular pump and probe beams.

3.2 Microcavity sample

Most of our measurements have been taken on high quality InGaAs-based microcavity wafers which show strong coupling below $T = 100\,\mathrm{K}$. These samples are by no means of the narrowest linewidth [27], but prove convenient because it is easy to match the spectral pulse-widths to their polariton linewidths. Many alternative designs of semiconductor planar heterostructure will produce strong coupling, but little difference in the dynamics is expected compared with the scheme presented here, as recently confirmed [20,28–30]. The cavity mirrors are fabricated from distributed Bragg reflectors (DBRs) of alternating transparent layers of different alloys of $Al_yGa_{1-y}As$, to produce a monolithic microcavity. The microcavity wafer grown here consists of two pairs of three $100\mathring{A}$ $In_{0.06}Ga_{0.94}As$ QWs in $100\mathring{A}$ GaAs barriers, sandwiched between 17 (20) pairs of DBRs $GaAs/Al_{0.18}Ga_{0.82}As$ on top (bottom). The optical cavity length is $\sim 3\lambda_x/2\sqrt{\varepsilon}$ and varies across the sample wafer allowing access to both positive and negative detunings, Δ. Careful angle-resolved spectroscopy has shown to be well fit by a transfer-matrix linear-propagation theory which uses the refractive index of each layer [31]. A slight splitting ($\sim 0.1\,\mathrm{meV}$) exists between TE and TM field polarizations due to the planar geometry however we will see that these splittings are overwhelmed by the spin selection rules of the QW excitons.

The lowest energy excitons in strained InGaAs quantum wells are derived from the heavy-hole valance bands, which have a spin $j_{hh} = \pm\frac{3}{2}$. Together with the electron spins $j_e = \pm\frac{1}{2}$ this produces two degenerate optical transitions of opposite circular helicity $j_x = \pm 1$. Excitation with right/left-circularly polarized light creates spin-up/down excitons respectively, and subsequent spin scattering can be dynamically tracked using time-delayed probe pulses (see Chapter 4). As we shall show in our results, near-resonant excitation of microcavities permits virtually no spin scattering. Spin is a good quantum number for polaritons, which implies that mixing with TE/TM photons and $j_x = \pm 2$ 'dark' excitons is not strong.

3.3 Parametric scattering

We now discuss pair-scattering in more detail as it turns out to dominate many of the nonlinear experiments. Two situations are of most interest, in which:

- polaritons injected at particular $k_\parallel$ can 'parametrically' scatter
- two excitons pair-scatter to produce a polariton in the trap

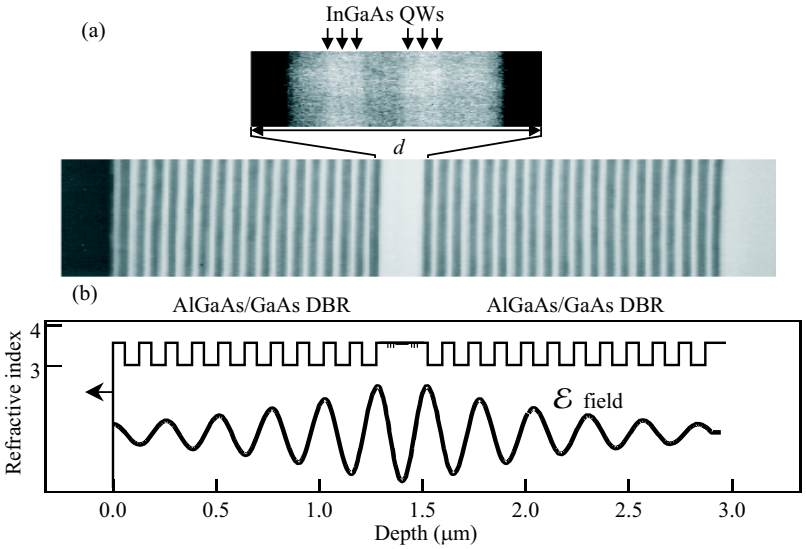

Fig. 8. (a) Microcavity sample cross-section: Scanning electron micrograph, with magnified QW region. (b) Refractive index profile of heterostructure layers, with the electric field distribution at the lower polariton resonant wavelength

Pulsed interactions

Parametric scattering (historically the first to be clearly identified experimentally [32]), can produce enormous optical nonlinearities of potential for ultrafast switching. On the other hand, exciton pair scattering (which was first to be identified theoretically [33]) is still under active investigation, with additional processes dominating those originally suggested [6,34].

In parametric scattering of polaritons, a laser beam incident at a particular angle injects a large population of polaritons at specific $k_{\|}$. Within the trap region these polaritons cannot easily lose energy, and only a small fraction make it to the polariton ground state. However at a particular 'magic' angle, $\boldsymbol{k} = \boldsymbol{k}_m$, two polaritons can parametrically scatter so that one ends up at $\boldsymbol{k} = 0$ and the other at $\boldsymbol{k} = 2\boldsymbol{k}_m$. The magic angle is given by the condition for energy and momentum conservation of the polariton dispersion, $2E(\boldsymbol{k}_m) = E(\boldsymbol{0}) + E(2\boldsymbol{k}_m)$ which leads to $\theta_m \simeq \sin^{-1}\{\sqrt{3\varepsilon\Omega\omega_x}\} \simeq 16.5°$. This process can be easily checked by probing the sample at normal incidence ($k = 0$) while scanning the angle and energy of a pump pulse along the polariton dispersion (Fig. 9). A clear resonance is seen at the predicted angle, whose effect is to produce substantial *gain* at the polariton ground state. This gain is

rather unexpected and different to that observed for equivalent experiments in semiconductor quantum wells. Normally as an electronic state becomes occupied, its absorption reduces because the ground state empties and the excited state fills, blocking further absorption (Fig. 9c). In semiconductors this is termed phase-space-filling, and is accompanied by comparably-large effects from exciton screening and exchange Coulomb terms. The saturation from phase space filling arises from the fermionic statistics of the semiconductor excitations. Something radically different occurrs for highly-populated polariton states.

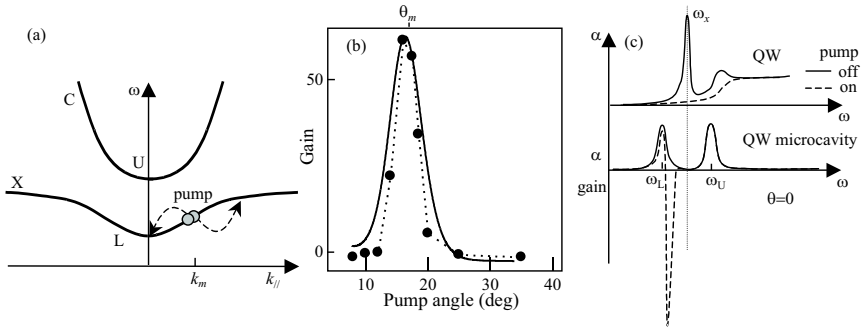

Fig. 9. (a) Parametric scattering between two pump photons at the magic angle. (b) Measured gain vs pump angle of incidence (c) linear and nonlinear absorption spectra for high power pumping of a QW and a microcavity containing the same QWs

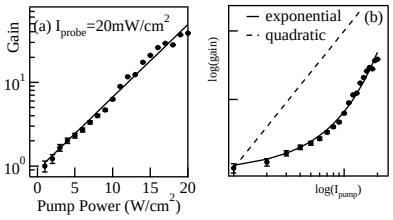

Fig. 10. Power dependence of the probe gain on (a) semi-log and (b) log plot, showing the exponential dependence of gain on pump power

By varying the pump power, just how different this polariton ground state is, becomes clear (Fig. 10). The exponential dependence of gain on pump power is a clear signature of a stimulated process. Occupation of the polariton ground state N_0 *increases* the scattering rate of polaritons into that state, $\frac{dN_0}{dt} \propto (1 + N_0)N_{k_m}$, hence the process accelarates until all available pump polaritons have been trapped or have decayed from the sample. This conclusion is backed up by a microscopic theoretical model which reproduces

all the experimental results [35,36]. The interaction driving the stimulated parametric scattering is once again the Coulomb interaction, V, between the electron and hole components of the exciton. This mixes polaritons at different places on the lower branch through an anti-Hermitian coupling,

$$\begin{bmatrix} \hbar\tilde{\omega}_L(0) & VN_{k_m} \\ -VN_{k_m} & \hbar\tilde{\omega}_L(2k_m) \end{bmatrix} \begin{bmatrix} |\hat{L}(0)\rangle \\ |\hat{L}^\dagger(2k_m)\rangle \end{bmatrix} = E \begin{bmatrix} |\hat{L}(0)\rangle \\ |\hat{L}^\dagger(2k_m)\rangle \end{bmatrix}. \tag{2}$$

The crucial negative sign in the off-diagonal mixing terms leads to an attraction between the two initially uncoupled polariton components, and the gain observed [36]. Although QW excitons (although nominally bosons) show predominantly the fermionic character of their constituents, the interacting polaritons behave as composite bosons. By mixing the exciton wavefunction together with a cavity photon, a new dispersion is produced which can use the Coulomb interaction for bosonic scattering at densities below those which access the underlying fermionic statistics of the electrons [37].

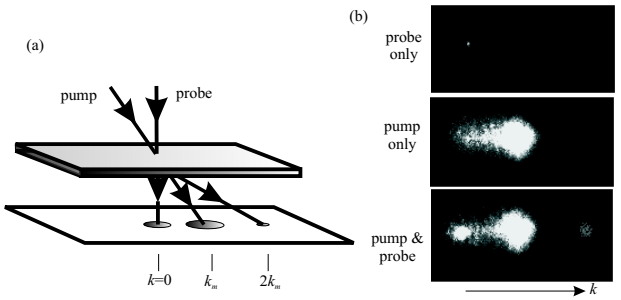

Fig. 11. Images of the emission from the microcavity when excited by pump at k_m and probe at $k = 0$, showing clearly the parametric scattering process

Both the polaritons in the trap ($k = 0$) and their high energy partners ($k = 2k_m$) have been observed in emission (Fig. 11). As the pump power is further increased it is possible to excite enough carriers and phonons to reach the fermionic regime at which point the strong coupling regime collapses [38]. Gains of up to $\sim 10^3$ occur at carrier densities well below that of all previous ultrafast semiconductor nonlinearities (peak powers here are below 10 kW) (Fig. 12). The gain in this quantum-engineered material can exceed $10^6\,\mathrm{cm}^{-1}$, higher than reported in any other substance, and yet still responding on ultrafast timescales. Injecting only a few aJ of energy along the sample normal produces a 30% change in the pump absorption in the sample. These nonlinearities are thus of great interest for all-optical switching and vertical-cavity amplifiers.

Even without injecting the probe pulse the total emission in the sample normal direction is superlinear in the pump power, indicating the presence of self-stimulation once a few polaritons have managed to scatter down to $k = 0$. This self-stimulation shows the strong tendency for polariton trapping to occur.

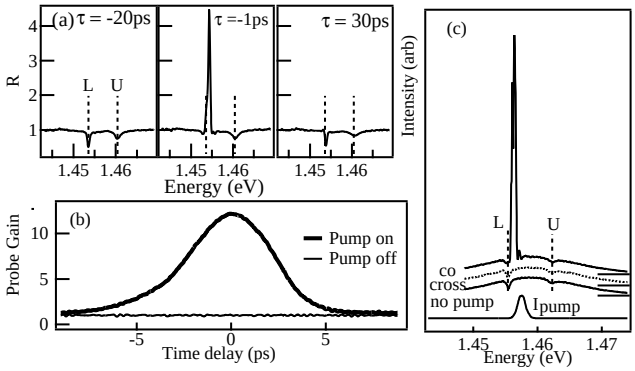

Fig. 12. (a) Reflection spectra measured by probe pulse at normal incidence arriving at indicated time delays relative to the pump pulse (injected at the magic angle). Gain is seen from polaritons in the trap (L). (b) Time-dependence of the reflectivity with the pump on/off. Reflectivites over 100% imply gain. (c) Probe spectra for co-circularly and cross-circularly polarised pump and probe pulses

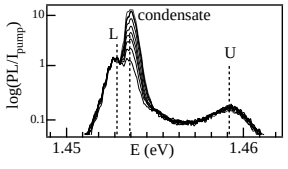

Fig. 13. Emission spectra as a function of pump intensity (normalised to the incident power) when only the pump pulse is injecting polaritons at $k = k_m$. Self-stimulated parametric scattering leads to the emergence of the new condensate line just above the lower polariton energy

CW interactions

Once the parametric scattering process was confirmed in pulsed measurements, it is clear it should also be apparent in CW resonant excitation at the same magic angle. Despite the main objection that with continuous excitation the background exciton population in the sample would rise sufficiently to collapse the strong coupling regime, we observe polariton pair-scattering overwhelming all other processes. Our experiments show that once the pump power at θ_m exceeds a few tens of mW, scattering into $k = 0$ totally dominates producing a beam of light in forward and backwards directions (Fig. 14a). As in the case of non-resonant parametric scattering in inorganic crystals inside a cavity, the resulting emission is a manifestation of an optical parametric oscillator (OPO). Two pump polaritons parametrically scatter to produce a 'signal' ($k = 0$) polariton which resonates inside the cavity and an 'idler' ($k = 2k_m$) polariton. Typical OPOs are > 1 cm long due to the weak parametric scattering strength - here we have shrunk the device by a factor of 10^4 through engineering a *resonant* parametric scattering. Our experiments

clearly show the expected behaviour of the output power, angular width, and resonant linewidth narrowing (Fig. 14b,c)[39].

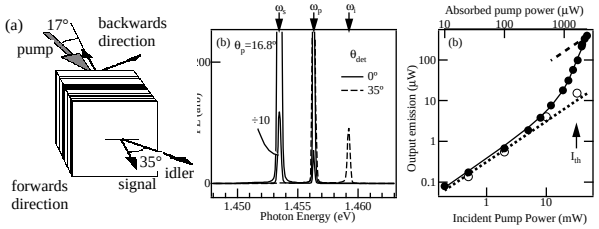

Fig. 14. (a) Schematic configuration of the microcavity OPO. (b) Emission spectra of signal and idler at $k = 0, 2k_m$ for CW pumping at $k = k_m$. (c) Pump power dependence of the signal emission, showing clear threshold behaviour

An alternative way to view this optically-pumped device depends on realising that a coherent macroscopic population of polaritons occupies the trap, each with an identical phase that is arbitrarily set by a spontaneous symmetry breaking. This is the description of a *polariton condensate*, which possesses coherence not just in the photon field (as in a laser) but also in the exciton fields. Such a state was predicted decades ago for bulk polaritons [10], and resembles a Bose-Einstein atomic condensate which is formed by evaporative-cooling of atoms until they are cold enough to condense. Here, the first few polaritons that scatter into the trap set the arbitrary phase for the further polaritons that they cooperatively stimulate to join them. Thus the condensate exists at a different energy and momentum to the reservoir of polaritons which efficiently feeds it, and is thus an example of a *non-equilibrium* condensate. It also differs from a laser in that an energy gap appears in the density of states [40]. Random variations in pump phase contribute only to the sum of the phase of the trapped populations since $\phi_s + \phi_i = 2\phi_p$. In contrast to superconductors which must be observed electrically, the signature of a polariton condensate is a strong beam of emerging light. The useful nature of the polariton condensate lies in its half-matter composition, which allows the manipulation of its phase. The phase of the polaritons is identical and their phase scattering is suppressed compared to excitons. Interferometric measurements of the polariton condensate linewidth show it to be $< 500\,\mathrm{MHz}$ (the resolution limit of our apparatus) and noise measurements suggest phase stability of several microseconds. By comparison to the Schalow Townes limit for lasers, the expected phase scattering $\propto \Gamma_0/N_0$ where the estimated occupation $N_0 \sim 10^4$ and the cavity decay rate $\Gamma_0 \sim (5\,\mathrm{ps})^{-1}$. This agrees well with our measurements and explains how the phase lifetime of single excitons

can be extended 10,000-fold by protecting them in large coherent polariton condensates.

Polariton Condensation

This brings us to the second scattering process of interest, which is between pairs of excitons. It is surprising that energetic excitons produced by the idler and which remain in the sample do not affect the parametric scattering. Our explanation is that these remaining excitons are too cold to give rise to much ionization of polaritons from the trap, and are relatively benign at low temperatures. For non-resonant excitation or at higher lattice temperatures, they can participate in exciton-polariton pair scattering releasing polaritons from the trap. Even so, recent predictions show the possibility of electrically-pumped microcavities working at room temperature [6].

To 'suck' polaritons into the trap requires excitons to lose energy to optic- or acoustic-phonon emission or through mutual Coulomb interactions (Fig. 6). Only an exciton with excess energy which is ω_{LO} above the polariton ground state can emit an LO phonon of specific wavevector to drop into the trap. Such processes have indeed been seen, but do not dominate in general since relatively few excitons are able to access this relaxation channel, and the scattering rate is small because the wavefunctions of the states are so different. Acoustic phonon emission into the trap is also extremely unlikely because this cannnot remove enough energy in a single scattering event [38]. The emission of light (through decay of the cavity photon component of the polariton) is thus predicted to be dominated by the non-equilibrium dynamics of polariton interactions, rather than by thermalisation with the phonon bath as is found for a population of excitons. Measurements of luminescence have shown this to indeed be the case [41]. The photoluminescence is predicted to depend sensitively on the photon energy and momentum used to excite the sample. The non-thermalised emission can even be asymmetric with respect to the sample normal, even though this is a planar sample geometry with a cylindrical symmetry (Fig. 15) [12].

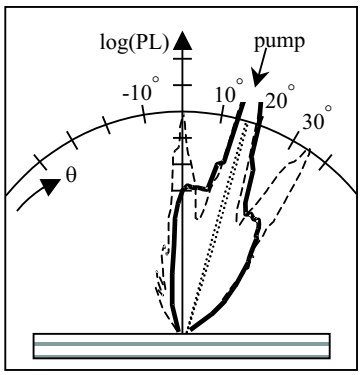

Fig. 15. Asymmetrical angular distribution of time-integrated PL (solid) and stimulated PL (dashed) when pumped by a pulse at the magic angle of 17° (dotted). Quantum well heterostructures show symmetrical emission

For two excitons at $\underline{k}_{1,2}$ in the exciton reservoir to exchange energy and momentum dropping one of the pair into the polariton trap, requires two specific conditions (Fig. 16): $\underline{k}_1 + \underline{k}_2 = \underline{k}_3$ and $\omega_1 + \omega_2 = \omega_L(0) + \omega_3$ with $\omega_i = \omega_X + \frac{\hbar|k_i|^2}{2M_x}$. This condition can be rewritten as a constraint on the original momenta

$$\frac{\hbar^2}{2M_x}\underline{k}_1.\underline{k}_2 = \hbar\Omega \tag{3}$$

which implies that the geometric mean of the exciton energies must equal the polariton trap depth. Only excitons which reach these high momenta can scatter into the trap, and only excitons which have nearly twice this momentum can ionize trapped polaritons. This sets the temperature and Fermi energies that control the density of the condensate ($k_BT, E_f > \hbar\Omega$),and suggests that it is indeed possible to electrically-pump polariton condensates providing that the excitons thermalise rapidly, and the trap is sufficiently deep [6,45]. Thus although our discussion of condensates involves optically-pumped samples at low temperatures, this is by no means a fundamental limitation for condensate technologies. Currently a number of groups are exploring GaN- and ZnSe-based semiconductor microcavities which are predicted to operate at room temperature. The extension of the vertical-cavity semiconductor laser (VCSEL) to the strong coupling domain no longer seems so remote.

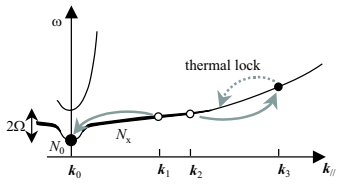

Fig. 16. Stimulated scattering process of exciton pairs from a thermal exciton population of N_x into the $k = 0$ condensate and higher energy exciton at k_3. The high energy exciton then relaxes back to thermal equilibrium preventing re-ionization of condensate polaritons

4 Condensate dynamics

Given that a polariton condensate can exist in semiconductor microcavities, with a phase lifetime which can potentially extend to μs or even ms, we can now discuss the manipulation of this state. Since our knowledge of these condensates is at a nascent stage, this section is more specifically an informed speculation. However the promise in each of these areas is considerable for quantum coherent manipulation and technologies.

4.1 Polariton interferometry

As with lasers, superconductors, atomic- and all other condensates, a clear possibility of interfering polariton condensates exists. Existing device imple-

mentations currently in use include Sagnac interferometers, superconducting interference devices (SQIDs), and atomic fountain gravitational detectors (Fig. 17). In each case, two condensates of fixed relative phase are created, either by a beamsplitter (light), Josephson junction (Cooper pairs) or by an optical standing wave beamsplitter (atoms). Interference occurs when the condensates are allowed to combine at a detector which can view the photon/current/atom fringes using a beamsplitter/ammeter/ionized particle counter (respectively). In each case, the phase difference accrued by the condensates in their different passage to the detector is measured, and this provides useful information about movement (Sagnac), magnetic fields (SQID) and gravity/frequency (atomic fountain). The extreme sensitivity of each of these interferometers comes from the phase stability of each condensate and the accuracy in counting many fringes which can reduce errors down to 1 part in 10^{12}. The excitonic component of polaritons is sensitive to magnetic and non-uniform electric fields, as well as gravity and temperature. Hence a number of all-solid-state polariton interferometers can be conceived.

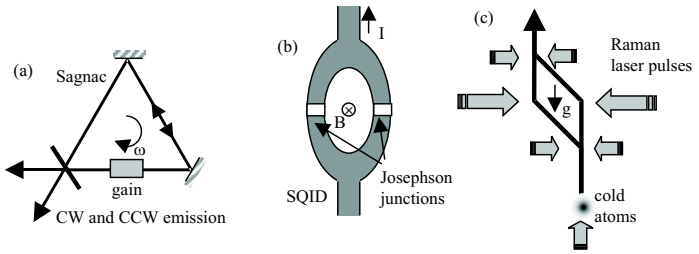

Fig. 17. Condensate interferometers: (a) Laser Sagnac interferometer detects angular accelarations by interfering counterpropagating laser beams (b) SQID Josephson junction superconducting devices detect magnetic fields in units of flux quanta trapped in the ring, and (c) atomic fountain gravitational accelarometers use laser beams to manipulate atoms

One possibility is to create polaritons at one location on a sample, spatially transport the polaritons through two physically-separated paths, and recombine them in a way that detects the local fringe pattern. Sermage *et al.*[42] have shown lateral propagation of polaritons travelling with the same in-plane momentum as originally injected, while our work shows that polaritons can diffuse several mm to regions of the sample which let photons escape (Fig. 18). Lateral transport of polaritons thus requires only that the lifetime of polaritons be sufficiently long to move them around. The main problem is that the flat dispersion around the bottom of the trap insists on *stationary* condensates, whereas a moving condensate is required. Our recent work on multiple condensates suggests that this is not a fundamental problem and condensates away from $k = 0$ are possible [36]. The energy loss rate of the condensate is sufficiently fast that the device would need to

be continuously (electrically or optically) pumped along its length, with the macroscopic phase set by the condensate component right up to the very edge of this layout. Possibly the greatest technological difficulty is growing microcavity samples in which the cavity thickness is sufficiently uniform that the resonant energy varies by less than the cavity linewidth across the interferometer length, however this is already the case for certain areas of the wafers. Such an interferometer laid out on a chip would be able to detect the effect of electric and magnetic fields on the internal motion of the exciton in a similar way to the internal phase sensitivity to gravity of atoms in an atomic fountain [43]. In comparison to laser interferometers, the phase coherent exciton component gives access to new environmental fields.

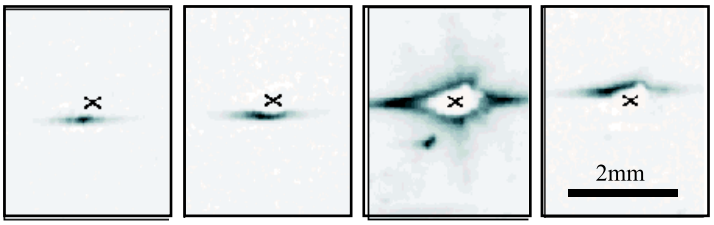

Fig. 18. Near field images of the sample emission when pumped with a pulsed pump at angle θ_m, which is focused at the point marked with an X. Frames from left to right correspond to increasing detuning of cavity and exciton $\Delta = -7, -3, 0, 3\,\mathrm{meV}$ and show diffusion of polaritons in the microcavity by $\sim 200\,\mu\mathrm{m}$

An alternative device model is based on temporal rather than spatial interferometry. We have so far avoided discussion of the spin of the polariton condensates, but it is this feature which has perhaps most potential. A circularly-polarized CW pump produces condensate emission which is completely co-circularly polarized. This fits with our model that parametric scattering is spin-preserving [Fig. 12(c)] [32]. When a linearly-polarized pump is used instead, the condensate emission polarization fluctuates on short timescales and is effectively unpolarized. We can see how this would occur by noting that linear-polarizations correspond to an equal superposition of right and left circular polarizations. Thus two condensates can form, one for each exciton spin, which posses independent macroscopic condensate phases, $\psi_{\uparrow,\downarrow}$ (Fig. 19). As their phase difference diffuses, so the resulting linearly-polarized emission randomly rotates with an orientation , $\theta_{poln} = \psi_{\uparrow} - \psi_{\downarrow}$. It is this condition of two co-located spin condensates that is so interesting, because it can be sensitive to local magnetic fields. The g-factor of excitons is rather small ($g_x \sim -0.5$ in InGaAs quantum wells of this width) so the splitting of excitons in weak magnetic fields is much less than the exciton linewidth and hard to measure (see Chapter 4). When a polariton condensate is used, the situation is rather different since the two spin condensates now exist at

slightly different energies $\hbar\Delta\omega = 2g_x\mu_B B$ which can be further apart than their small linewidths due to the condensate phase scattering rate. Detection of the emission would reveal sinusoidal beats as the two condensates evolve in and out of phase - simple measurement of this MHz beat frequency provides the local magnetic field. Estimates of the current phase lifetime lead to magnetic field sensitivity below $100\,\mu$T, compared to typically 1 T fields normally applied to split excitons. Ring geometries (see below) may be used to improve this sensitivity.

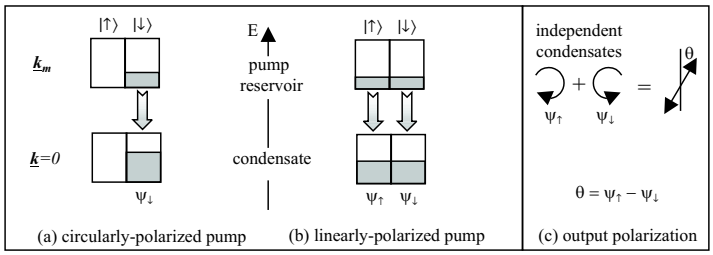

Fig. 19. Spin-dependent polariton occupations with (a) circularly-polarized pump producing circularly-polarized condensate (b) Linearly-polarized pump producing two oppositely circularly-polarized condensates of different phase ψ resulting in (c) varying linear polarization θ

Experiments are currently in progress to demonstrate the feasibility of polariton spin interferometry. In atomic laser systems this scheme is rather complicated because such spin-split two-mode lasers tend to compete for optical gain from the single pump reservoir. For semiconductor microcavities a separate reservoir exists for each condensate and, in the absence of phase locking of the condensates (for example produced by strain in the sample), the two condensates are stable. Many additional questions can also be posed such as the influence of nuclear spins in the sample (Chapter 4).

4.2 Macroscopic quantum states

Although many theories of semiconductors are based on the idea of delocalised plane wave electronic states, no semiconductor system yet exists in which a particular wavefunction can be addressed from different spatial locations (Fig. 20). A system of this kind is needed for matter-wave tests of quantum measurement such as EPR-type correlation and entanglement. Recently a number of groups have been using near-field microscopy on samples with quantum well disorder produced by interrupting the growth, to try to identify excitonic wavefunctions which have a length-scale $> 100\,$nm and thus (in principle) simultaneously addressable at different locations. Similar ideas have prompted local electrical probing of the phase of mesoscopic supercon-

ducting islands. The complexity and difficulty of such experiments leads us to suggest an alternative route employing polariton condensates.

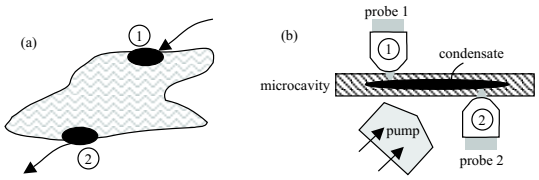

Fig. 20. (a) Macroscopic coherent state allows spatially-separated disturbance and measurement at particular times. (b) Realisation for polariton condensate probed from different sides of the sample

Condensates have a size set by the finesse of the microcavity, the parametric scattering rate and the polariton condensate density [36,39]. In the current realization, both far-field and near-field imaging show that the 50 μm diameter of the condensate is independent of the pump focus diameter, and dependent only on the cavity finesse. Using microscope objectives placed on either side of the sample it is possible to access much smaller regions of the condensate and probe their entanglement and dynamic response. For instance, if a weak probe pulse of specific phase is injected into one part of the condensate, how long does it take for this perturbation to propagate across the macroscopic quantum state? Can the individual polaritons in a condensate be located? Answering such normally-inaccessible questions is helpful for building robust intuitions to develop new quantum technologies.

As a first test of such ideas we apply the analogy between polaritons and Cooper pairs to measure Josephson coupling between two polariton condensates. Two CW pump beams excite the sample from opposite sides at the same magic angle of 16°, with the same in-plane momentum. Independent control of each pump polarization and focal spot allows condensates of variable separation and spin to be excited. We find evidence of spin-dependent interactions in the near-field emission for spin parallel and antiparallel condensates (Fig. 21). The total emission (at normal incidence) increases as the condensates overlap. However the data is complicated by further spin-dependent interactions to be discussed elsewhere [44]. These first experiments show the potential for spatially-dependent condensate interactions.

A final example of wavefunctions sensitive to spatial coherence are the higher order Airy modes of the microcavity. We first note that although the transverse modes of the empty microcavity are Airy modes, they are substantially altered by the strong coupling regime. The polariton ground state corresponds to the $l = 0$ mode and it is possible to excite higher order transverse modes in the cavity, as occasionally seen in vertical-cavity surface-emitting lasers (VCSELs). However instead of the $\mathrm{TEM}_{10,01,11}$ modes recorded from such electrically-pumped mesas, it is possible to excite lasing ring modes in semiconductor microcavities. We have observed such behaviour

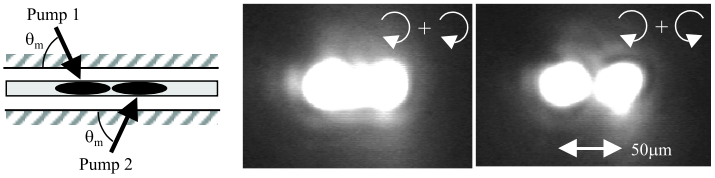

Fig. 21. Two condensates pumped by circularly-polarised CW beams of equal intensity incident from the front and back of the sample at θ_m. The near-field images show the difference between spin-parallel and spin-antiparallel condensates in close proximity

(Fig. 22) for near-resonant selective pumping, also discussed in detail elsewhere [45]. Ring modes can be used to carry angular momentum with each Airy mode labelled by the total angular momentum l (integral) and spin projection $m_l = 0, \pm 1, ..., \pm l$ [46]. Laser beams with these spatial profiles form micro-rings when brought to a focus, however these have not yet been exploited in the study of semiconductors. This is because although there is optical coherence between points on opposite sides of the ring, there is no electronic coherence - the electronic wavefunctions excited are separately localised and are not quantum-mechanically correlated. When considering the interaction of such a laser beam with a polariton condensate this is no longer true, and it should be possible to impart a specific angular momentum to the excited condensate. In analogy with magnetic vortices trapped in mesoscopic superconducting disks, we predict a panoply of electric field vortices that can exist in the polariton condensate. Such states should be sensitive to the sign of a magnetic field threading the condensate. Similarly it should be possible to use angularly-polarized pump and probe beams (together with spin polarization) to create novel coherent states in these systems. The phase stability of such states should be particularly high and suggest the possibility of creating spatially-entangled wavefunctions.

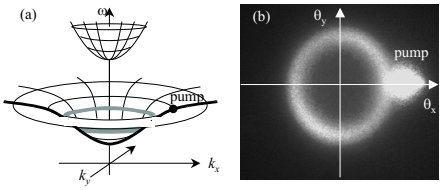

Fig. 22. (a) Different excitation conditions can enable optically-pumped lasing in higher order Airy modes, producing (b) ring emission seen imaged on a screen next to the sample

4.3 Quantum-correlated pairs

The parametric process that creates pairs of signal and idler polaritons is responsible for additional quantum-correlations, which exist between the pho-

tons emitted from these modes in different directions [47]. Some of the most sensitive tests of Bell's inequalities have used parametric downconversion from pump photons at 2ω to produce quantum correlated signal and idler at sideband frequencies $\omega \pm \epsilon$ [48,49]. Quantum cryptography typically relies on such a process to distribute quantum ciphers, however the extreme inefficiency of this conversion often mandates high intensity pulsed sources to drive single-photon pulses.

The resonant parametric scattering process in microcavities is 10^4 times more efficient, but a number of problems need to be addressed before exploitation is possible. The first is that signal polaritons at $k = 0$ are much more likely to be reradiated than the idler polaritons at $k = 2k_m$ which can scatter into much higher k exciton states [12]. One solution is to use a different configuration of laser beams, with the pump incident at the bottom of the polariton trap at $k = 0$ and quantum correlations measured between signal and idler photons at $k = \pm q$. A second problem is that the quantum correlations are much reduced by the choice that polaritons have to randomly decay into either forward or backward directions. By suitably engineering the DBR mirrors in the heterostructure it is possible to suppress optical emission from the top of the sample, and restore the strong quantum correlations. A number of groups are currently actively pursuing this arrangement [50,51].

4.4 Conclusions

The possibilities listed so far by no means exhaust the range of quantum technologies that can be accessed through the polariton condensate. Many other prospective states are yet to be explored in this rich system such as spin waves and other collective excitations, quantum bistability and spatial solitons, pseudo-spin in double microcavities, and spin transport using inhomogeneous electric fields. Mapping potentially interesting investigations will pave the way for a new generation of solid-state quantum technologies in strongly-coupled light-matter systems. Much can be learned from the basic principle of using the coupling of fully-engineered wavefunctions to create quasiparticles with new properties. In the present realization this provides a way for Coulomb interactions to introduce a new long-lived coherent state in semiconductors. Such ideas are applicable to a wide variety of other systems including organic chromophores such as J-aggregates, liquid crystals, and even nanostructured metals.

5 Acknowledgements

Grateful thanks to the constant enthusiasm and skill of experimentalists: Pavlos Savvidis, Maurice Skolnick, Mark Stevenson, Pavlos Lagoudakis, Caterina Netti; theorists: David Whittaker, Alexei Kavokin and helpful comments from colleagues Dave Hanna, Anne Tropper and Monique Combescot.

6 References

References

1. N.H. Bonadeo et al.: Science **282** 1473 (1998)
2. F. Schmidt-Kaler G. Rempe and H. Walter: Phys. Rev. Lett. **64**, 2783 (1990)
3. M.O. Scully and M.S. Zubairy:*Quantum Optics* (CUP, Cambridge 1997)
4. G. Khitrova et al.: Rev. Mod. Phys. **71**, 1591 (1999)
5. M.S. Skolnick, T.A. Fisher and D.M. Whittaker: Semicond. Sci. Tech **13**, 645 (1998)
6. J.J. Baumberg: Phys. Rev. Lett., submitted (2001)
7. F. Yura and E. Hanamura: Phys. Rev. B **50**, 15457 (1994)
8. B. Honerlage, R. Levy, J.B. Grun, C. Klingshirn, and K. Bohnert: Phys. Rep. **124**, 161 (1985); S. Savasta and R. Girlanda: Phys. Rev B **59**, 15409 (1999)
9. J.J.Hopfield and D.G. Thomas: Phys. Rev. **132**, 563 (1963); F. Evangelisti, F.U. Fishbach and A. Frova: Phys. Rev. B **9**, 1516 (1974)
10. L.V. Keldysh: 'Macroscopic coherent states of excitons in semiconductors'. In *Bose-Einstein Condensation*. ed. by A. Griffin, D.W. Snoke, S. Stringari (CUP, Cambridge 1995) pp. 246–281
11. J.J. Baumberg, A.P. Heberle, A.V. Kavokin, M.R. Vladimirova, and K. Köhler: Phys. Rev. Lett. **80**, 3567 (1998)
12. P.G. Savvidis, J.J. Baumberg et al.: Phys. Rev. B **62**, R13278 (2000)
13. S. Schmitt-Rink, D. S. Chemla, and D. A. B. Miller: Adv. in Phys. **38**, 89 (1989)
14. S. Schmitt-Rink and D. S. Chemla: Phys. Rev. Lett. **57** 2752, (1986)
15. S. Schmitt-Rink, D. S. Chemla, and H. Haug: Phys. Rev. B **37**, 941 (1988)
16. H. Haug and S. W. Koch: *Quantum Theory of the Optical and Electronic Properties of Semiconductors* (World Scientific, Singapore 1993)
17. F. Jahnke, M. Kira and S.W. Koch: Z. Phys. B Cond. Mat **104**, 559 (1997)
18. A.I. Tartakowskii et al.: Phys.Rev. B **62**, R2283 (2000)
19. A. Ishikawa C. Weisbuch, M. Nishioka and Y. Arakawa: Phys. Rev. Lett.**69**, 3314 (1992)
20. P. Senellart and J. Bloch: Phys. Rev. Lett. **82**, 1233 (1999)
21. R. Houdré, C. Weisbuch, R.P. Stanley, U. Oesterle, and M. Ilegems: Phys. Rev. Lett. **85**, 2793 (2000)
22. Le Si Dang et al.: Phys. Rev. Lett. **81**, 3920 (1998)
23. R. Huang, F. Tassone, Y. Yamamoto: Phys. Rev. B**61**, R7854 (2000)
24. F. Tassone and Y. Yamamoto: Phys. Rev. B**59**, 10830 (1999)
25. M.Kuwata-Gonokami et al.: Phys. Rev. Lett. **79**, 1341 (1997)
26. J.J. Baumberg: 'Coherent Control and Switching'. In *Semiconductor Quantum Optoelectronics*. ed by A. Miller, M. Ebrahimzadeh and D.M. Finlayson(IOP, Bristol, 1999) pp. 100–117
27. F. Quochi et al.: Phys. Rev. Lett. **80**, 4733 (1998)
28. J. Erland et al.: phys. stat. sol. (b)**221**, 115 (2000)
29. G. Dasbach et al.: Phys. Rev. B **62**, 13076 (2000)
30. F. Boeuf et al.: Phys. Rev. B **62** R2279 (2000)
31. D. Baxter: *Semiconductor Microcavities* PhD thesis, (Sheffield University, Department of Physics, 1998)
32. P.G.Savvidis, J.J. Baumberg et al.: Phys.Rev.Lett.**84**, 1547 (2000)

33. A. Imamoglu et al.: Phys. Rev. A **53** 1996, (1996)
34. B. Sermage P. Senellart, J. Bloch and J.Y. Marzin: Phys. Rev. B **62**, R16263 (2000)
35. C. Ciuti et al.: Phys. Rev. B **62**, R4825 (2000)
36. P.G. Savvidis, C. Ciuti, J.J. Baumberg et al., Phys. Rev. B bf ??, ??? (2001)
37. O.W. Greenberg and R.C. Hilborn, Phys. Rev. Lett **83**, 4460 (1999)
38. R.M. Stevenson et al.: Phys.Rev.Lett. **85**, 3680 (2000)
39. J.J. Baumberg et al.: Phys. Rev. B**62**, R16247 (2000)
40. P.R. Eastham and P.B. Littlewood, arXiv:cond-mat/0102009 (2001)
41. U. Oesterle R. Houdre R.P. Stanley, S. Pau and M. Ilegems: Phys. Rev. B **55**, R4867 (1997)
42. T. Freixanet et al.: Phys. Rev. B **61** 7233 (2000)
43. M. Kasevich and S. Chu: Phys. Rev. Lett. **67**, 181 (1991)
44. P. Lagoudakis et al.: Phys. Rev. B, submitted (2001)
45. P.G. Savvidis et al.: Phys. Rev. Lett., submitted (2001)
46. N.B. Simpson, K. Dholakia, L. Allen and M.J. Padgett: Opt. Lett. **22** 52 (1997)
47. A.M. Fox, J.J. Baumberg et al.: Phys. Rev. Lett. **74**, 1728 (1994)
48. J.G Rarity and P.R.Tapster: Phil. Trans. Roy. Soc. Lond. A **355**, 2267 (1997) and references therein
49. Z.Y. Ou and L. Mandel: Phys. Rev. Lett. **61**, 50 (1988)
50. S.Savasta S and R. Girlanda: Phys. Rev. B **59**, 15409 (1999)
51. G. Messin et al.: J. Phys. Cond. Matt. **11**, 6069 (1999)